Journal of Alloys and Compounds 805 (2019) 1034–1043

Contents lists available at ScienceDirect

Journal of Alloys and Compounds

journal homepage: http://www.elsevier.com/locate/jalcom

Suppressed voltage decay and improved electrochemical performance by coating $LiAl_5O_8$ on the surface of $Li_{1.2}Mn_{0.54}Ni_{0.13}Co_{0.13}O_2$

Fang Yang [a], Shengzeng Lin [a, *], Zhimeng Guo [a], Yanru Shao [a], Biao Zhang [a], Xiaodong Zhang [a], Shuhao Yan [a], Alex A. Volinsky [b]

[a] Institute for Advanced Materials and Technology, University of Science and Technology Beijing, Beijing, 100083, China
[b] Department of Mechanical Engineering, University of South Florida, Tampa, FL, 33620, USA

ARTICLE INFO

Article history:
Received 19 March 2019
Received in revised form
16 June 2019
Accepted 17 June 2019
Available online 18 July 2019

Keywords:
Lithium-rich
$LiAl_5O_8$ coating
Layered oxides
$Li_{1.2}Mn_{0.54}Ni_{0.13}Co_{0.13}O_2$

ABSTRACT

$LiAl_5O_8$-coated $Li_{1.2}Mn_{0.54}Ni_{0.13}Co_{0.13}O_2$ cathode materials were synthesized by using the co-precipitation method along with a facile sol-gel coating process. Homogeneous and 3–5 nm thin $LiAl_5O_8$ film was formed on the LMNC surface. After the coating modification, discharge specific capacity, the initial Coulombic efficiency, and rate performance were improved to some extent. It was particularly important to note that the voltage decay of the battery after the charge and discharge cycle was well suppressed. Specifically, the 3 wt% $LiAl_5O_8$-coated electrode can deliver the initial discharge capacity of 243.5 mAh g^{-1} with a low irreversible capacity loss of 51.1 mAh g^{-1} and the initial Coulombic efficiency reached the maximum of 82.63% at 0.1 C rate. Although the 1 wt% $LiAl_5O_8$-coated electrode was cycled through 100 cycles at a rate of 0.5 C, the capacity retention rate was still up to 95.8%, while that of the $LiAl_5O_8$-free one was only 82.8%. The stable and thin $LiAl_5O_8$ coating layer protected the electrode structure from HF corrosion and other side reactions and reduced the oxygen loss (in the form of Li_2O) by suppressing the initial activation of Li_2MnO_3.

1. Introduction

In recent years, lithium-ion batteries have found wide applications in electric vehicles, large-scale grid energy storage, and mobile electronic devices, etc. [1–5]. In the current lithium battery material system, the negative electrode basically uses lithium intercalation materials such as graphite, and its capacity is much larger than that of various commercial cathode materials, and the energy density of the current lithium ion battery depends on the cathode material used. At present, various types of cathode materials with the largest amount of use have various problems. For example, the cobalt element in $LiCoO_2$ is expensive and toxic, which makes it difficult to obtain a large-scale use of a cathode material having a high cobalt content [6]. $LiFePO_4$, as a positive electrode material for power batteries, has certain advantages in terms of safety and cost, but its lower theoretical specific capacity (160 mAh g^{-1}) makes it impossible for pure electric vehicles to obtain sufficient cruising range [7]. In recent years, the ternary system cathode material ($LiNi_xCo_yMn_{(1-x-y)}O_2$) that has been highly praised can reach a specific capacity of up to 200 mAh g^{-1}, but it is still difficult to meet the needs of electric vehicles for longer cruising range [8,9]. Therefore, it is necessary to develop a cathode material system with low cost and high specific capacity.

As a new type of cathode material, lithium-rich material can provide a specific capacity of more than 250 mAh g^{-1} at a rate of 0.1 C discharge. Since its constituent elements are mainly low-cost manganese elements, it has a greater advantage in terms of raw material costs than current ternary materials [10,11]. It is well known that the current most lithium-rich cathode materials are mainly composed of a monoclinic layered phase Li_2MnO_3 and a trigonal layered phase $LiMO_2$ [3,12–14]. Among various Li-rich materials, $Li_{1.2}Mn_{0.54}Ni_{0.13}Co_{0.13}O_2$ (LMNC) has relatively good stability while maintaining large discharge capacity. However, the lithium-rich cathode materials currently studied generally still have problems such as voltage cycle decay, low charge and discharge efficiency in the first cycle, and poor rate performance, leading to the delay in large-scale market application [13,15,16]. At present, numerous reports have been presented on the mechanisms of cyclic decay of lithium-rich cathode electrodes. Thereinto, electrode/electrolyte interface degradation, gas production, and

* Corresponding author.
E-mail address: linsz0908@163.com (S. Lin).

https://doi.org/10.1016/j.jallcom.2019.06.208
0925-8388/

transition metal dissolution are thought to be the main factors [17]. It is well known that during cycling, the liquid electrolyte reacts with an electrode material, thereby destroying the original structure of the electrode material, and resulting in deterioration of the cycle performance of the battery. In addition, the formation of hydrofluoric acid (HF) in the electrolyte is considered to have a devastating effect on the cycle performance because it can accelerate Mn and Ni dissolution from the LMNC bulk [18,19].

To overcome these issues, numerous efforts have been employed to improve the electrochemical performance of Li-rich materials, including elements doping strategy [5,20,21], surface coating modification [13,15,22–25], particle size control [26–28], morphology optimization [2] and high-temperature treatment [29]. Thereinto, surface coating modification is considered to be the most simple and effective method.

$LiAl_5O_8$ (lithium aluminate oxide, LAO) with the space group 213 is commonly used as fluorescent material [30,31], and it is a promising coating candidate with excellent structural stability in organic electrolyte [32]. Using $LiAl_5O_8$ as the coating modifier can block direct contact between the positive electrode material and the organic electrolyte to avoid layer structure damage caused by excessive metal dissolution.

Therefore, it is of interest to employ $LiAl_5O_8$ on the LMNC surface to improve the electrochemical performance. In this study, the LMNC particles were coated with $LiAl_5O_8$ by the sol-gel method. To date, no related reports have been presented regarding this subject. Besides, the $LiAl_5O_8$ effect on microstructure, electrochemical properties of the LMNC cathode in LIBs was also investigated in detail.

2. Experimental procedure

2.1. Samples preparation

First, the $(Mn_{0.54}Ni_{0.13}Co_{0.13})CO_3$ was synthesized by a coprecipitation method. Specifically, nickel sulfate hexahydrate (Guizhou Dalong Huicheng New Material Co., Ltd., China), Cobalt sulfate heptahydrate (Guizhou Dalong Huicheng New Material Co., Ltd., China), manganese sulfate monohydrate (Jilin Jien Nickel Industry Co.,Ltd., China), and sodium carbonate (Sinopharm Chemical Reagent Co., Ltd., China) were used as the raw materials to prepare 0.5 L 1.0 mol L^{-1} MSO_4 and 0.5 L 1.0 mol L^{-1} Na_2CO_3 solution. Both solutions were simultaneously dropped into a continuous stirring reactor at 55 °C. Simultaneously, ammonia as a chelating agent was employed to adjust the pH of the mixed solution to 7.5–8.5. After that, the temperature was kept for 2 h, and then the co-precipitation carbonate precursor was filtered several times and vacuum dried. Subsequently, stoichiometric amounts of $(Mn_{0.54}Ni_{0.13}Co_{0.13})CO_3$ and Li_2CO_3 (a mole ratio of Li/metal ions was equaled to 1.05:1) were mixed and fully grinded in an agate mortar. Finally, the mixture was first preheated at 500 °C for 5 h and then annealed at 850 °C for 10 h with a heating rate of 5 °C/min in the air.

The second step was to prepare the $LiAl_5O_8$-coating layer on the $Li_{1.2}Mn_{0.54}Ni_{0.13}Co_{0.13}O_2$ surface. The process of $LiAl_5O_8$ modification by the sol-gel method is shown in Fig. 1. A calculated amount of $LiNO_3$, $AlNO_3 \cdot 9H_2O$, and urea were dissolved in 10 mL deionized water to prepare a premixed solution. The as-prepared $Li_{1.2}Mn_{0.54}Ni_{0.13}Co_{0.13}O_2$ powder was added into the premixed solution for sonication with a holding time of 0.5 h, and then the stirring was carried out at 60 °C in the water bath until a gel was formed. Finally, the obtained gel was dried overnight at 80 °C followed by being calcined at 750 °C for 2 h with a heating rate of 5 °C/min in the air. For comparison, pure $LiAl_5O_8$ was also prepared under the same conditions.

2.2. Characterization

The phase composition and crystal structure of the synthesized samples were identified by X-ray diffraction (XRD, TTRIII) with Cu Kα radiation. The scanning rate was 5° min^{-1}, and the scanning range of the diffraction angle (2θ) was 10–90°. Microstructure analysis was conducted by scanning electron microscopy (SEM, LEO-1450). The field emission scanning electron microscope (FESEM, Zeiss Supra55) equipped with energy dispersive spectroscopy (EDS) was employed to analyze the composition distribution. Microstructural characterization of the prepared samples was performed by transmission electron microscopy (TEM, Tecnai G2 F30 S-TWIN).

2.3. Electrochemical measurements

In order to test the electrochemical performance of the prepared active materials, all samples were fabricated into CR2032 coin-type haft cells in Ar-filled glove box. The positive cathode consisting of 80 wt% as-prepared active materials powers, 10 wt% polyvinylidene fluoride (PVDF), and 10 wt% acetylene black, was dispersed to N-methyl-2-pyrrolidone (NMP) solvent to prepare the black slurry. Then, the slurry was uniformly applied to the rough surface of the aluminum foil with a blade. The electrolyte was 1 M $LiPF_6$ dissolved in a mixture of ethylene carbonate (EC)/dimethyl carbonate (DEC)/ethyl methyl carbonate (EMC) (1:1:1 vol ratio). The lithium metal and Cellgard 2400 polypropylene film acted as the negative electrode and separator, respectively. The battery charge and discharge

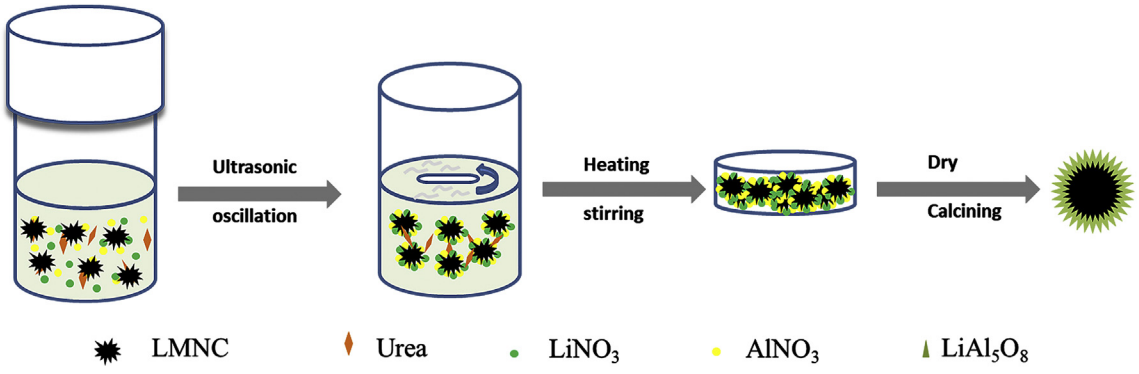

Fig. 1. Schematic illustration of the synthesis of $LiAl_5O_8$-coated LMNC samples.

test was conducted on a battery test system (Land CT2001A, Wuhan Jinnuo Electronic Co. Ltd) between 2 V and 4.8 V (vs. Li^+/Li) at ambient temperature. The current density of 250 mA g^{-1} was defined as the 1 C rate during the test. Electrochemical impedance spectroscopy (EIS) experiments were carried out using the CHI600E electrochemical workstation in the frequency range of 0.1 MHz to 0.01 Hz with an AC perturbation signal of 5 mV to research the kinetics of different samples.

3. Results and discussion

3.1. Materials characterization

To ensure the phase composition of synthesized $LiAl_5O_8$, XRD analysis was carried out. As shown in Fig. 2a, the $LiAl_5O_8$ phase can be formed compared to the standard PDF card. However, the corresponding diffraction reflections were not sharp, indicating that an amorphous phase was formed or incomplete crystallization occurred. Besides, the XRD patterns of the pristine and $LiAl_5O_8$-coated LMNC samples are presented in Fig. 2b. All the diffraction lines were indexed on the hexagonal α-$NaFeO_2$ layered structure with the space group of R3(_)m. A small set of diffraction peaks appeared in the region of 20–23°, which was the orderly arrangement of Li and Mn in the Li_2MnO_3 ($Li[Li_{1/3}Mn_{2/3}]O_2$) component in a small range. The structure of the Li_2MnO_3 ($Li[Li_{1/3}Mn_{2/3}]O_2$) component is attributed to the monoclinic structure of the space group C2/m type [33]. The distinct splitting of (006)/(012) and (018)/(110) also indicated the well-developed layered structure. However, the third phase wasn't detected, which can be ascribed to the low concentration or amorphous structure of the $LiAl_5O_8$ phase [4,34].

Table 1 lists the lattice parameters of all samples and the ratio of I(003)/I(104) diffraction reflections intensities. Corresponding to different $LiAl_5O_8$ content varying from 0 wt% to 5 wt%, the intensity ratio of I(003)/I(104) ranged from 1.37 to 1.49 (>1.2). The I(003)/I(104) value is typically employed to represent the degree of cation mixing and it is widely believed that the layered material suffers a low degree of cation mixing when the ratio is beyond 1.2 [35]. Both the high ratio of I(003)/I(104) and obvious splitting of (006)/(012) and (018)/(110) can indicate that the active material possessed a well-crystallized layered structure with hexagonal ordering (O3 type) [12]. It was worth noting that the lattice parameter c of modified samples increased to varying degrees compared to that of pristine LMNC. This may be related to the partial diffusion of the Al atoms into the bulk of LMNC [34,36].

Table 1
Structure parameters of pristine and LiAl5O8 coating samples analyzed from XRD patterns.

Samples	$I_{(003)}/I_{(104)}$	a (Å)	c (Å)	c/a
LMNC	1.37	2.853	14.168	4.966
LAO-1	1.43	2.846	14.220	4.996
LAO-3	1.49	2.849	14.185	4.98
LAO-5	1.48	2.849	14.200	4.984

3.2. Morphology and structure of the pristine and $LiAl_5O_8$-coated $Li_{1.2}Mn_{0.54}Ni_{0.13}Co_{0.13}O_2$

SEM images and EDS patterns of elements identification of pristine and 3 wt% $LiAl_5O_8$-coated samples are presented in Fig. 3. The LMNC secondary particles were nearly spherical or ovate with a diameter of 5–15 μm, consisting of nanoparticles with a diameter of 150–500 nm. There was no obvious difference in morphology between pristine LMNC and $LiAl_5O_8$-coated LMNC samples under low and medium magnifications. However, under high magnification, the surface of the LAO 3 wt%-coated sample was somewhat rough and fuzzy, as shown in Fig. 3e. It can be inferred that the amorphous $LiAl_5O_8$ coating layer was attached on the particle surface. As shown in Figs. 3f–g, the EDS elemental analysis of pristine and $LiAl_5O_8$-coated samples proved that the synthesized samples were in good agreement with the target products. To further demonstrate whether the elements were evenly distributed and $LiAl_5O_8$ was uniformly coated on the LMNC surface, the elemental distribution was also conducted. As shown in Fig. 4b–f, Ni, Co, Mn and O elements were mainly dominant in the LMNC phase. It was worth noting that Al element was evenly distributed on the surface of the particle, indicating that the $LiAl_5O_8$ was successfully coated on the surface of the LMNC particles.

HRTEM and corresponding Fast Fourier Transform (FFT) analysis was performed to further investigate the microstructure characteristics of the pristine and 3 wt% LAO-coating samples. As shown in Fig. 5a–c, the FFT pattern and lattice fringes of the inner region of the LMNC show that the LMNC phase was successfully formed, and the lattice had a plane spacing of 0.472 nm, which corresponded to the d-spacing of the (003) planes of the layered R3m phase of LMNC. Comparing Fig. 5a with Fig. 5d, it can be found that the edges of the particle without coating modification were smooth and flat, while a thin coating layer was observed in the edges of the sample modified by the 3 wt% LAO. It can be clearly seen in Figs. 5e–f that the LAO coating layer was uniformly coated on the surface of the

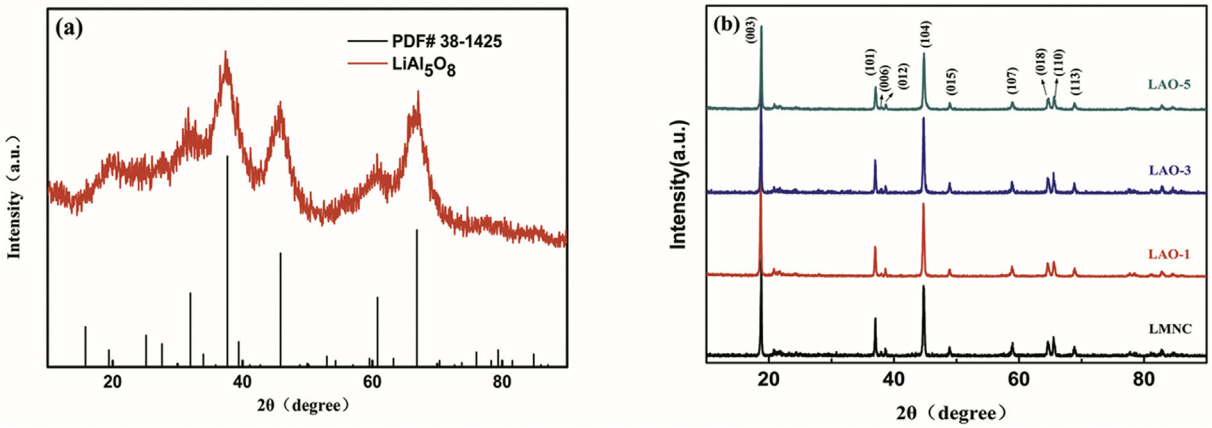

Fig. 2. XRD patterns of: (a) pure $LiAl_5O_8$, (b) pristine and $LiAl_5O_8$-coated LMNC.

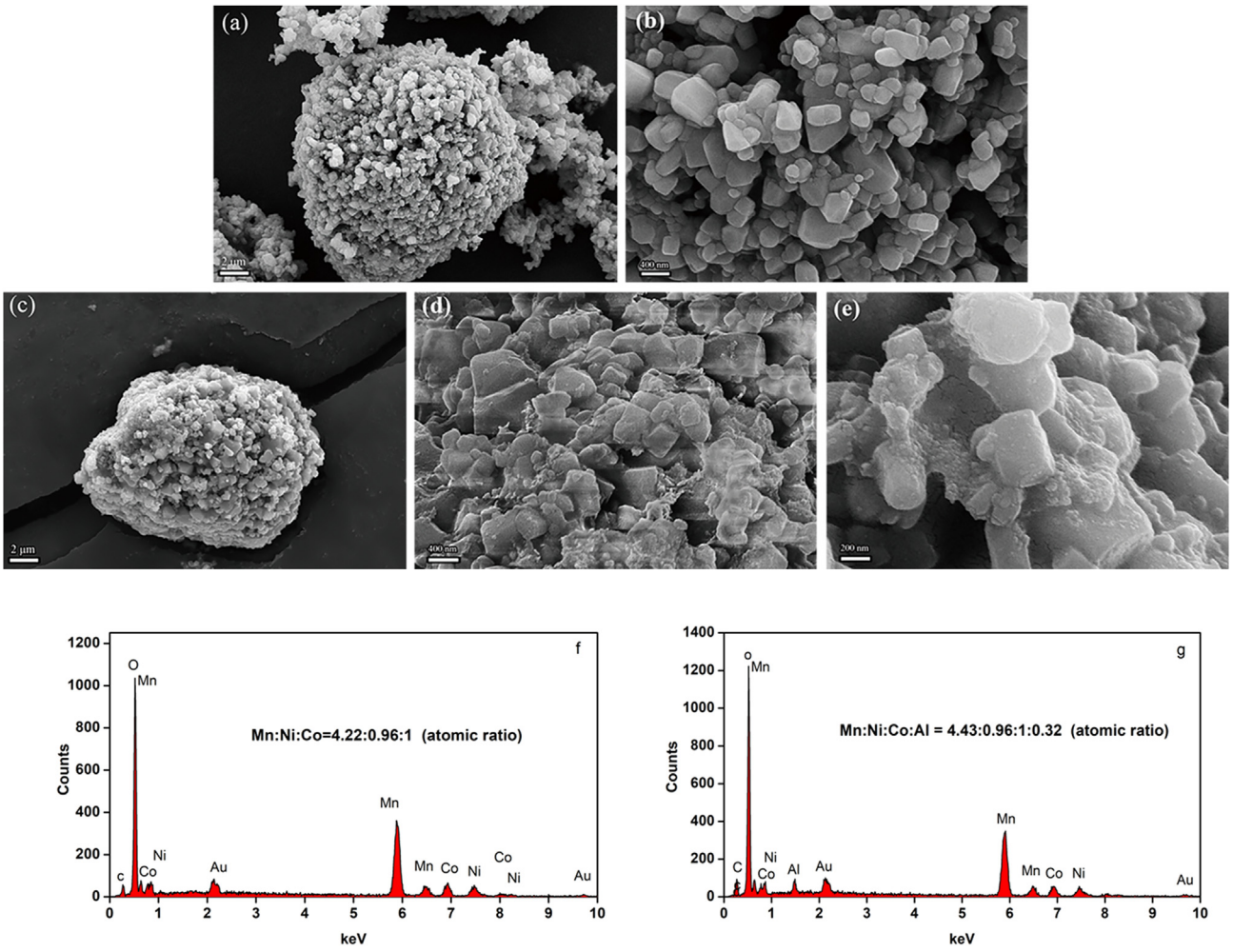

Fig. 3. SEM images of pristine and $LiAl_5O_8$-coated samples: (a, b) pristine LMNC, (c, d, e) $LiAl_5O_8$-3 wt.%, and (f, g) EDS patterns of elements identification of pristine and $LiAl_5O_8$-3 wt.%.

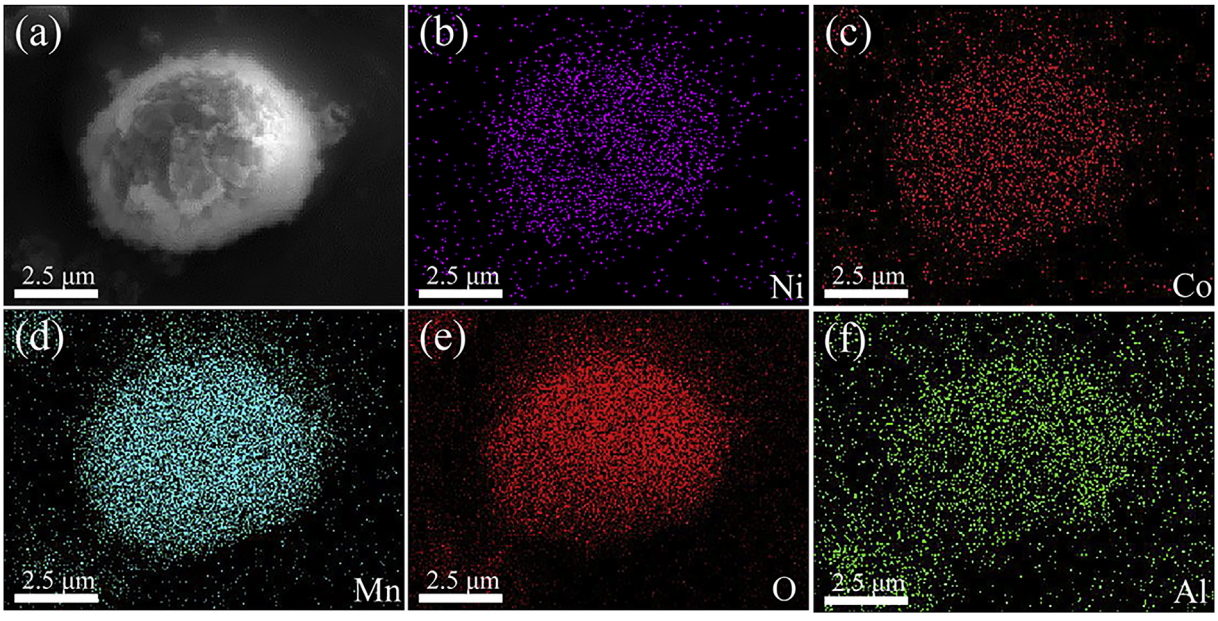

Fig. 4. (a) FESEM image, and element distribution of (b) Ni, (c) Co, (d) Mn, (e) O, and (f) Al in the $LiAl_5O_8$-3 wt.% LMNC.

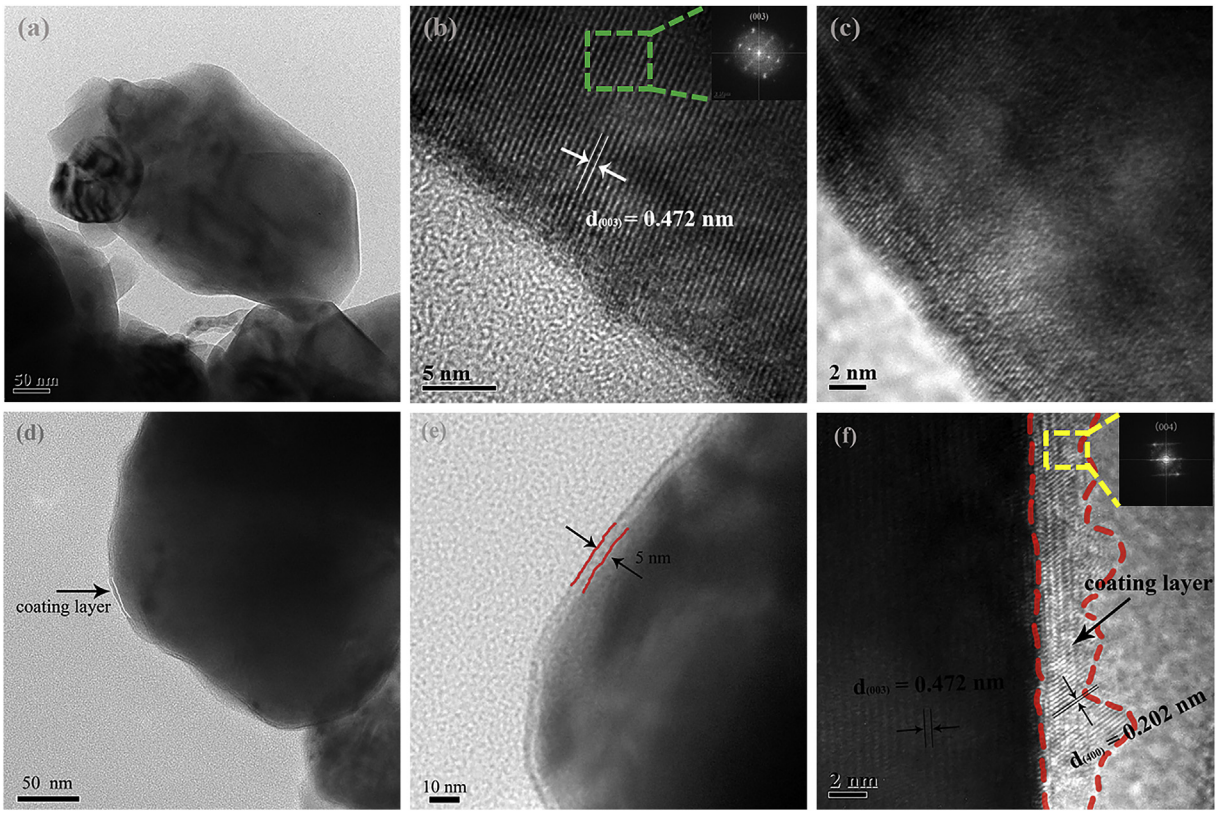

Fig. 5. HRTEM and corresponding Fast Fourier Transform images of (a, b, c) pristine, and (d, e, f) $LiAl_5O_8$-3 wt.% coated LMNC.

LMNC bulk particles with a thickness of about 3–5 nm. The chemical composition of the formed LAO coating layer was also proven by the EDS analysis. The formation of uniform LAO coating on the LMNC surface was beneficial to protect the active materials from directly contacting with the electrolyte and being attacked by HF in the electrolyte [32]. Thus, the presence of the LAO-coating layer would allow voltage decay to be suppressed during cycling.

3.3. Electrochemical performance

Fig. 6 shows the initial charge and discharge curves of the pristine LMNC and the modified material at a constant current density of 0.1 C (1 C = 250 mAg^{-1}) between 2 V and 4.8 V at ambient temperature. All of the samples exhibited typical dual-platform characteristics of lithium-rich materials during the first cycle of charging, which was consistent with the related literature reports [21,22,37,38]. As shown in Table 2, the pristine LMNC delivered a relatively higher charge capacity of 353.7 $mAhg^{-1}$, while the modified samples showed a lower charge capacity of 343.7 $mAhg^{-1}$, 294.6 $mAhg^{-1}$, and 332.1 $mAhg^{-1}$, respectively. This was most likely due to the presence of the LAO coating, which affected the release of Li^+ and O^{2-} (as Li_2O) extracted from the Li_2MnO_3-like lattice, resulting in a decrease in charge capacity after the voltage reached 4.5 V or higher [38,39]. There was a slight increase in the discharge capacity of LAO-coating modified LMNC compared with the pristine samples. Consequently, the Coulombic efficiency was significantly improved after the surface coating modification. The optimal electrochemical performance was achieved in the 3 wt% coated samples. This was the reason why only the microstructure analysis of 3 wt% coated samples was carried out for comparison with the pristine samples.

In order to further understand the electrochemical reaction

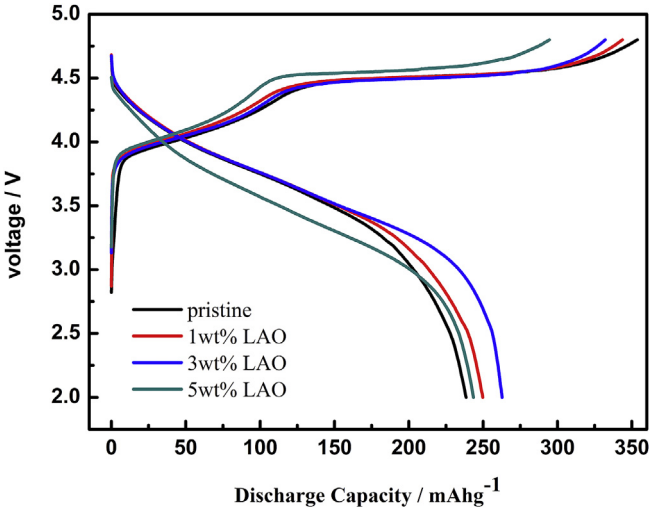

Fig. 6. Initial charge/discharge profiles of LMNC and $LiAl_5O_8$-coated LMNC electrodes between 2 V and 4.8 V at a constant current density of 0.1 C.

occurred during the initial charge/discharge process and analyze the reasons of changes in charge/discharge capacity, the differential charge-discharge capacity (dQ/dV) profiles of selected cycles are presented in Fig. 7. It can be found in Figs.7a and c that the two samples behaved similar, with two distinct oxidation peaks at around 4 V and 4.5 V in the initial charge process. The first one is mainly due to the delithiation accompanied with the oxidation of Co^{3+} and Ni^{2+} [24], while the latter one can be attributed to the irreversible loss of oxygen from the lattice of Li_2MnO_3-like accompanied with the formation of the layered active MnO_2

Table 2
The first charge/discharge capacity, irreversible capacity and initial Coulombic efficiency values for the pristine and surface-modified samples at 0.1 C.

Samples	Charge ($mAhg^{-1}$)	Discharge ($mAhg^{-1}$)	Loss ($mAhg^{-1}$)	Coulomb efficiency (%)
LMNC	353.7	238.5	115.2	67.43
LAO-1	343.7	249.7	94	72.64
LAO-3	294.6	243.5	51.1	82.63
LAO-5	332.1	262.7	69.4	79.12

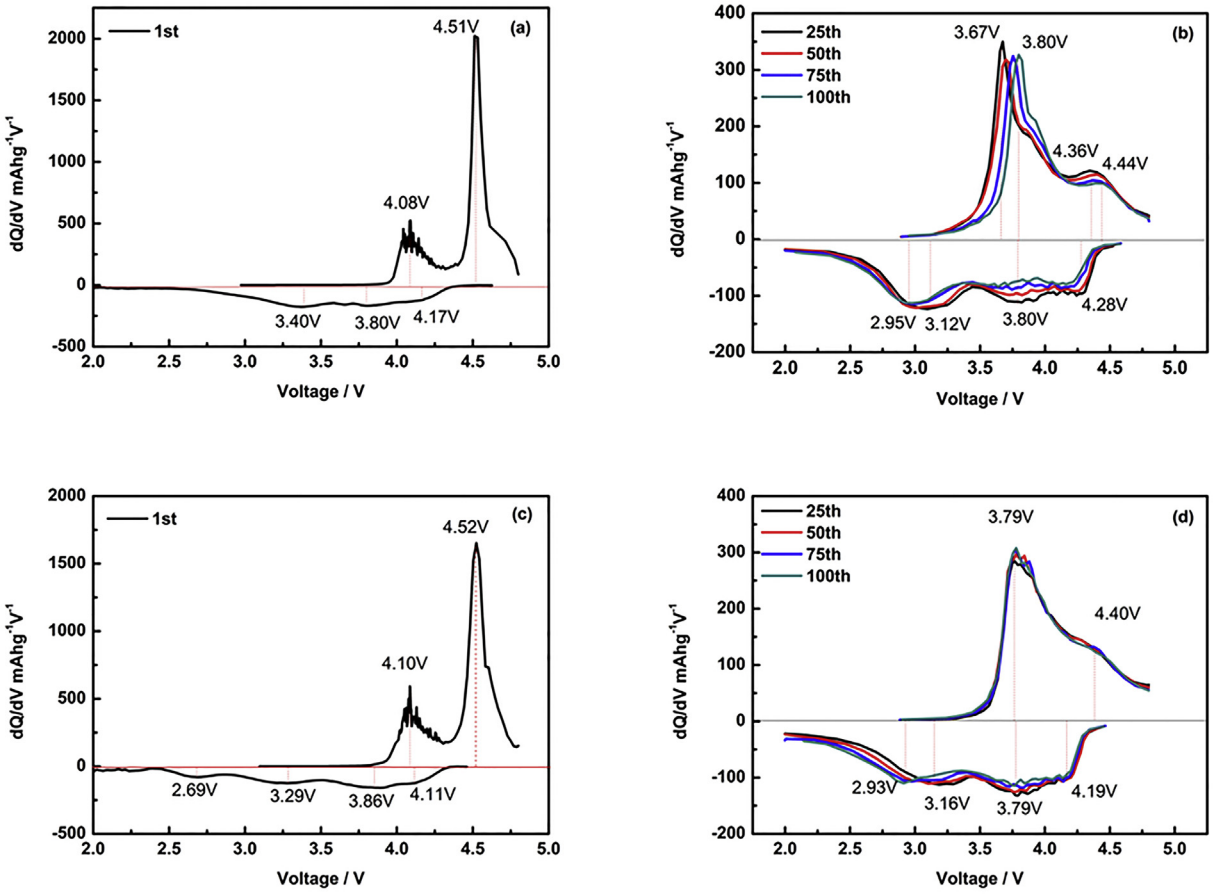

Fig. 7. dQ/dV profiles of (a, b) pristine LMNC, and (c, d) 3 wt% $LiAl_5O_8$-coated LMNC.

[16,40]. As the number of cycles increased, the oxidation peak and the reduction peak of the pristine LMNC moved to the positive and negative directions, respectively. However, the corresponding peak of the LAO-3 basically remained unchanged, which indicated that the polarization in the charging process can be reduced by the $LiAl_5O_8$ coating to a certain extent. For the first discharge process, as shown in the insets of Figs. 7a and c, three obvious reduction peaks were observed at around 4.2 V, 3.8 V and 3.4 V. The first two peaks corresponded to the reduction of Ni^{4+} and Co^{4+} and the last one was attributed to the lithiation of the layered active MnO_2. However, compared with the pristine LMNC, the LAO-3 sample exhibited an additional reduction peak at 2.7 V, probably due to the formation of the spinel phase. The amount of the spinel was so small that it could not be detected by the XRD analysis.

Fig. 8a displays the cycling performance of the pristine and $LiAl_5O_8$-coated LNNC at a rate of 0.5 C after activation for five cycles at a rate of 0.1 C. The corresponding discharge capacity values are listed in Table 3. The capacity retention rate of the modified material improved to some extent. Compared with the capacity retention rate of 82.8% of the pristine LMNC, the capacity retention rate of the coated LMNC with 1 wt% $LiAl_5O_8$ reached the maximum of 95.8% after 100 cycles. It was worth noting that the discharge specific capacity was fluctuated after $LiAl_5O_8$ coating. This phenomenon was mainly due to the influence of different amounts of $LiAl_5O_8$ on the embedding of Li^+ in the process of discharge. Specifically, the charging process of lithium battery corresponded to the lithium ion stripping from the positive electrode, while the discharge process was contrary to the process of lithium ion embedding into the positive electrode. After the original cathode material was coated with $LiAl_5O_8$, a small number of lithium ions were retained on the negative electrode or $LiAl_5O_8$ surface in the process of charge and discharge, and failed to be embedded in the layered cathode material at the end of part of the cycle. This part of the lithium ion may be embedded in the positive electrode in the next cycle, resulting in an increase in the discharge specific capacity during the cycle, while the previous cycle capacity was slightly lower, namely the discharge specific capacity fluctuation phenomenon. At present, voltage attenuation is a thorny issue in the use of lithium-rich cathode materials. As shown in Fig. 8b, voltage fading clearly occurred in the pristine LMNC, which may be caused

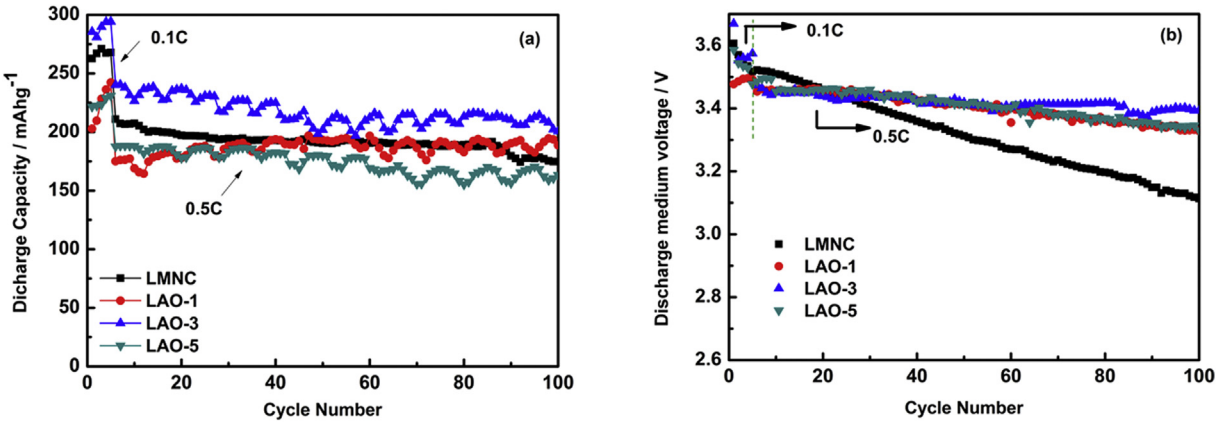

Fig. 8. (a) Cycle performance at 0.5 C and (b) discharge mid-point voltage profiles of pristine LMNC and $LiAl_5O_8$-coated LMNC.

Table 3
The discharge capacity values for the pristine and surface-modified LMNC samples at 0.5 C rate.

sample	Discharge Capacity at 0.5 C			
	The 6th cycle ($mAhg^{-1}$)	Maximum ($mAhg^{-1}$)	100th cycle ($mAhg^{-1}$)	Capacity retention (%)
LMNC	211	211	174.7	82.8
LAO-1	175.1	196.9	188.7	95.8
LAO-3	240.2	240.4	200.7	83.5
LAO-5	187.5	188.2	163.3	86.8

by the structural change of the electrolyte reacting with the positive electrode material during the cycle. However, more obvious voltage fading was observed in the pristine LMNC compared to the modified samples. Due to the structural complexity of Li-rich materials, the mechanism of voltage decay is still not well understood. Yu et al. [16] believed that the voltage decay phenomenon of Li-rich materials was related to the activation of low-voltage redox couples such as Mn^{3+}/Mn^{4+} and Co^{2+}/Co^{3+} due to the oxygen release of the material during cycling. The use of the coating modification means is a method for effectively suppressing the harmful side reaction between the positive electrode material and the electrolyte to protect the positive electrode material. It should be pointed out that the traditional Al_2O_3 coating modification can improve the performance of the cathode material to a certain extent, but the Al_2O_3 coating is used as an absorbent of HF to achieve the mission of protecting the cathode material. Unfortunately, with the depletion of Al_2O_3, this protection will also fail. $LiAl_5O_8$ has excellent chemical stability against HF attacks, and it is evenly covered on the surface of the positive electrode material, thus protecting it from harmful substances such as HF during long-term use. Therefore, the presence of $LiAl_5O_8$ coating layer not only prevented the direct contact of the active LMNC material with the electrolyte, but also suppressed the release of oxygen and the loss of Li^+ (Li_2O), which in turn made it difficult to activate the low voltage pair and suppressed the formation of the new phase in the bulk. Consequently, the voltage decay phenomenon during the cycle can be inhibited and the overall Li-rich layered framework got maintained.

Fig. 9 shows the rate capability of the four samples at various current density varied from 0.1 C to 2 C. With the current density increase, the discharge capacity of all samples gradually decreased. Especially at medium and high rates of 1 C and 2 C, the discharge capacity decreased sharply, which revealed the poor rate performance of Li-rich materials. However, it was worth noting that all the $LiAl_5O_8$-coated samples had a better rate performance of varying degree. Thereinto, the capacity delivered by pristine LMNC was about 113 $mAhg^{-1}$ at the rate of 2 C, while the value delivered

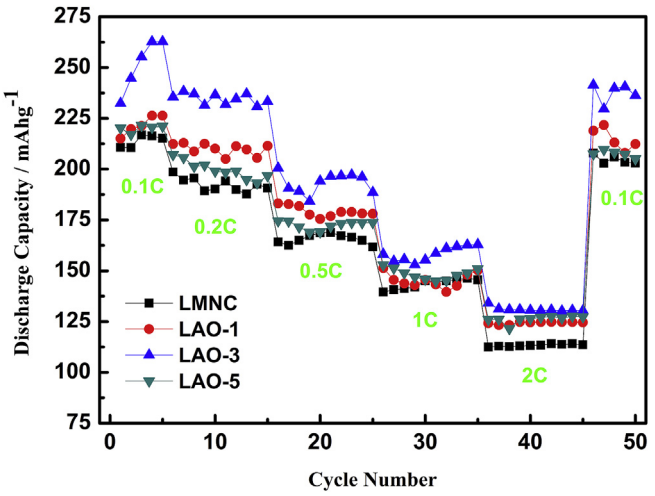

Fig. 9. Rate performance at various C-rates from 0.1 C to 2 C.

by the LAO-3 samples was up to 131 $mAhg^{-1}$. When the current rate was re-dropped to 0.1 C, the LAO-3 samples still showed significant advantages over other samples. This was supposedly due to the appropriate thickness of $LiAl_5O_8$ film, which can hinder the direct reaction between the cathode surface and electrolyte, resulting in the reduction of the thickness of the SEI film during the cycle and the easier transfer of lithium ions. In addition, the presence of the $LiAl_5O_8$ layer may also provide additional transmission channels for lithium ions to transport between the particle surface and the electrolyte. The above results indicated that the introduction of an appropriate amount of $LiAl_5O_8$ coating layer was beneficial.

In order to study the effect of the $LiAl_5O_8$ coating on the electrochemical kinetics of the bulk LMNC, EIS testing was performed on all samples, the EIS samples included two parts: one was placed for 12 h after being assembled, the other was cycled at 0.5 C for 100

Table 4
Fitted impedance parameters of pristine and $LiAl_5O_8$-coated LLNMO at different cycles.

Cycle number	0th		100th		
Sample	R_s (ohm)	R_{ct} (ohm)	R_s (ohm)	R_f (ohm)	R_{ct} (ohm)
LMNC	2.125	432.2	2.793	11.04	3459
LAO-1	1.669	275.3	3.401	14.2	2116
LAO-3	1.714	225.4	3.211	26.19	1933
LAO-5	2.769	405.2	2.879	16.56	3718

cycles. The corresponding EIS test fitting values and Nyquist plots are listed in Table 4 and Fig. 10, respectively. As seen in Figs. 10a–b, the impedance spectra of before cycling consisted of a semicircle in the high frequency region and a diagonal line in the low frequency region, and the impedance spectrum after 100 cycles was mainly composed of two semicircles in the high frequency region and the intermediate frequency region. The semicircle in the high frequency region (expressed by the symbol R_f) represented the interfacial film resistance which was related to the interfacial film resistance [solid electrolyte interface (SEI)]. And the semicircle in the intermediate frequency region (expressed by the symbol R_{ct}) represented charge interfacial capacitance and transfer resistance at the electrode/electrolyte interface, while the sloping line at the low frequency region (marked as W_1) associated with the Warburg impedance representing lithium-ion diffusion in the electrode bulk [4,25,34].

As shown in Table 4, there was not much difference in the R_s values before the cycle, with a range of 1.669–2.769 Ω, which was corresponding to the combined resistance of the electrolyte, Li metal anode and the Al foil current collector [41,42]. After 100 cycles, the value increased slightly, ranging from 2.793 Ω to 3.401 Ω. The R_{ct} values of all sample were similar before cycling, and the difference between each R_{ct} value was relatively small. Nevertheless, after 100 cycles, the R_{ct} value of pristine sample increased from 432.2 Ω to 3459 Ω, while that of the LAO-3 sample only increased from 225.4 Ω to 1933 Ω. This data indicated that the $LiAl_5O_8$ coating layers can suppress the interface side reactions between the cathode and electrolyte to reduce the interfacial resistance. These results matched well with the improved electrochemical properties of the LAO-3 samples.

At the same time, the SEM images of LAO-3 coated LMNC electrode and the pristine LMNC electrode after 100 charge and discharge cycles were obtained to further explore the effect of $LiAl_5O_8$ coating on the stability of LMNC electrode. As shown in Fig. 11, the $LiAl_5O_8$ coated samples basically retained the complete

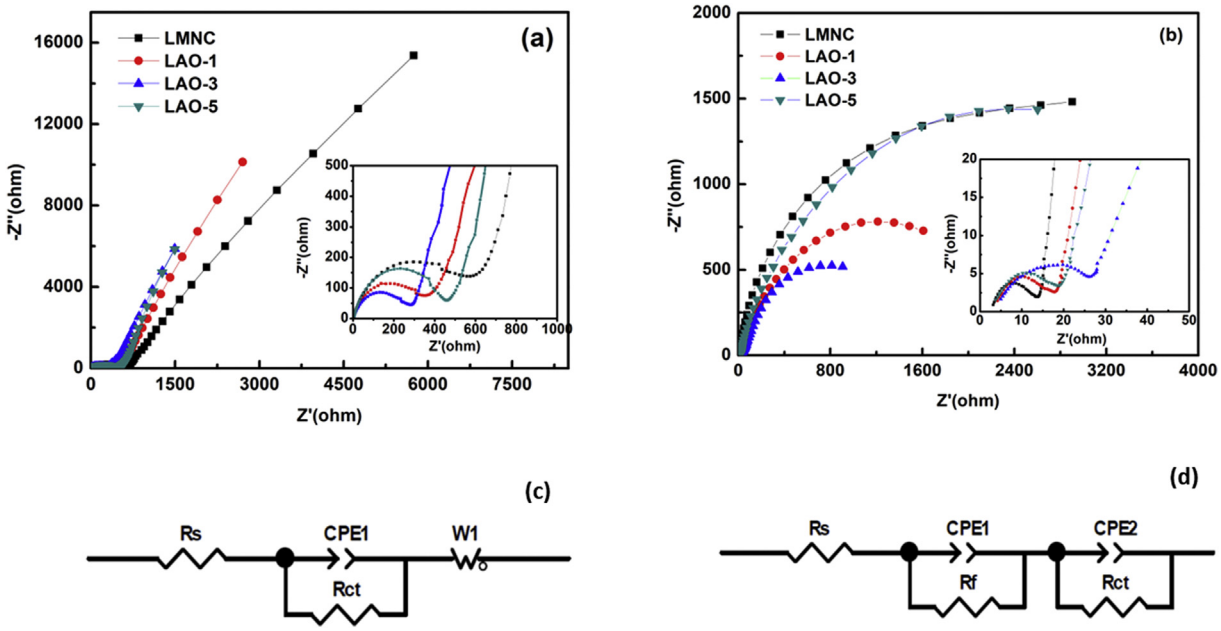

Fig. 10. EIS plots of pristine and $LiAl_5O_8$-coated LMNC samples and the corresponding equivalent circuit model: (a, c) before cycling, and (b, d) after 100 cycles at 0.5 C.

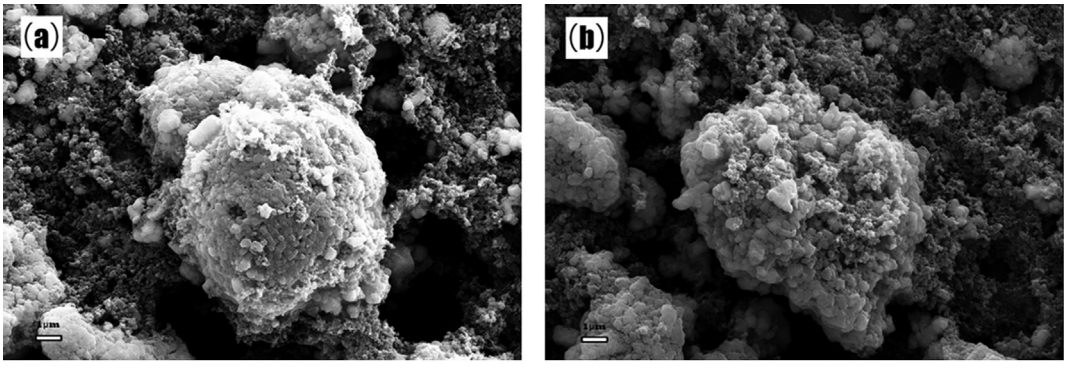

Fig. 11. SEM images of (a) $LiAl_5O_8$-coated LMNC samples and (b) pristine after 100 cycles at 0.5 C.

spherical particle morphology, and there was no obvious collapse and rupture. On the contrary, after the circulation of pristine samples, there was a serious collapse deformation. This phenomenon can be attributed to the attack of HF and the release of oxygen in high saturation state, which also leaded to the rapid increase of R_{ct} and the deterioration of cycling ability and thermal stability [34,41]. The appearance of this phenomenon was consistent with the results of EIS test. The results showed that $LiAl_5O_8$ coated LMNC electrode could reduce the side effect damage caused by HF attack and delay the release of oxygen.

4. Conclusions

In summary, $LiAl_5O_8$-coated $Li_{1.2}Mn_{0.54}Ni_{0.13}Co_{0.13}O_2$ cathode materials were successfully synthesized via a sol-gel method. The optimal $LiAl_5O_8$ content was 3 wt% and an obvious 3–5 nm coating layer was observed on the LMNC particle surface. In the 3 wt% $LiAl_5O_8$-coated $Li_{1.2}Mn_{0.54}Ni_{0.13}Co_{0.13}O_2$ samples, excellent reversible capacity, enhanced cycling ability, and better rate capability were obtained, as compared to the pristine one. After coating modification, the structural stability of LMNC was enhanced, and the voltage decay phenomenon during the cycle was significantly suppressed. This improvement can be ascribed to the $LiAl_5O_8$ coating layer protecting the electrode structure from destruction.

Conflicts of interest

There are no conflicts to declare.

Acknowledgments

This study was funded by the China Postdoctoral Science Foundation (No. 2018M641188), the Fundamental Research Funds for the Central Universities (No. FRF-TP-18-025A1) and the National Key R&D Program of China (No. 2016YFB1101201).

Appendix A. Supplementary data

Supplementary data to this article can be found online at https://doi.org/10.1016/j.jallcom.2019.06.208.

References

[1] W.M. Seong, K.-Y. Park, M.H. Lee, S. Moon, K. Oh, H. Park, S. Lee, K. Kang, Abnormal self-discharge in lithium-ion batteries, Energy Environ. Sci. 11 (2018) 1–24.
[2] L. Chen, Y. Su, S. Chen, N. Li, L. Bao, W. Li, Z. Wang, M. Wang, F. Wu, Hierarchical Li1.2Ni0.2Mn0.6O2 nanoplates with exposed {010} planes as high-performance cathode material for lithium-ion batteries, Adv. Mater. 26 (2014) 6756–6760.
[3] H. Yu, H. Zhou, High-energy cathode materials (Li_2MnO_3-$LiMO_2$) for lithium-ion batteries, J. Phys. Chem. Lett. 4 (2013) 1268–1280.
[4] W. Liu, X. Li, D. Xiong, Y. Hao, J. Li, H. Kou, B. Yan, D. Li, S. Lu, A. Koo, K. Adair, X. Sun, Significantly improving cycling performance of cathodes in lithium ion batteries: the effect of Al_2O_3 and $LiAlO_2$ coatings on LiNi0.6Co0.2Mn0.2O2, Nano Energy 44 (2018) 111–120.
[5] H. Yu, H. Zhou, Initial Coulombic efficiency improvement of the Li1.2Mn0.567Ni0.166Co0.067O2 lithium-rich material by ruthenium substitution for manganese, J. Mater. Chem. 22 (2012) 15507.
[6] K.S. Tan, M.V. Reddy, G.V.S. Rao, B.V.R. Chowdari, High-performance $LiCoO_2$ by molten salt (LiNO3:LiCl) synthesis for Li-ion batteries, J. Power Sources 147 (2005) 241–248.
[7] T.K. Fey, K.P. Huang, H.M. Kao, W.H. Li, A polyethylene glycol-assisted carbothermal reduction method to synthesize $LiFePO_4$ using industrial raw materials, J. Power Sources 196 (2011) 2810–2818.
[8] C. Nithya, V.S. Kumari, S. Gopukumar, Synthesis of high voltage (4.9 V) cycling LiNixCoyMn(1-x-y)O2 cathode materials for lithium rechargeable batteries, Phys. Chem. Chem. Phys. 13 (2011) 6125–6132.
[9] K. Okada, N. Machida, M. Naito, T. Shigematsu, S. Ito, S. Fujiki, M. Nakano, Y. Aihara, Preparation and electrochemical properties of $LiAlO_2$-coated Li(Ni(1/3)Mn(1/3)Co(1/3))O2 for all-solid-state batteries, Solid State Ion. 255 (2014) 120–127.
[10] M.M. Thackeray, S.H. Kang, C.S. Johnson, J.T. Vaughey, R. Benedek, S.A. Hackney, Li_2MnO_3-stabilized $LiMO_2$ (M = Mn, Ni, Co) electrodes for lithium-ion batteries, J. Mater. Chem. 17 (2007) 3112–3125.
[11] J.S. Kim, C.S. Johnson, J.T. Vaughey, M.M. Thackeray, S.A. Hackney, W. Yoon, C.P. Grey, Electrochemical and structural properties of xLi2M`O3·(1−x) LiMn0.5Ni0.5O2 electrodes for lithium batteries (M`=Ti, Mn, Zr; $0 \le x \le 0.3$), Chem. Mater. 16 (2004) 1996–2006.
[12] L. Zhang, N. Li, B. Wu, H. Xu, L. Wang, X.Q. Yang, F. Wu, Sphere-shaped hierarchical cathode with enhanced growth of nanocrystal planes for high-rate and cycling-stable li-ion batteries, Nano Lett. 15 (2015) 656–661.
[13] X.D. Zhang, J.L. Shi, J.Y. Liang, Y.X. Yin, J.N. Zhang, X.Q. Yu, Y.G. Guo, Suppressing surface lattice oxygen release of Li-rich cathode materials via heterostructured spinel $Li_4Mn_5O_{12}$ coating, Adv. Mater. 30 (2018), 1801751.
[14] F. Wu, Q. Li, L. Bao, Y. Zheng, Y. Lu, Y. Su, J. Wang, S. Chen, R. Chen, J. Tian, Role of $LaNiO_3$ in suppressing voltage decay of layered lithium-rich cathode materials, Electrochim. Acta 260 (2018) 986–993.
[15] D. Ma, P. Zhang, Y. Li, X. Ren, Li1.2Mn0.54Ni0.13Co0.13O2-encapsulated carbon nanofiber network cathodes with improved stability and rate capability for Li-ion batteries, Sci. Rep. 5 (2015) 11257.
[16] E. Hu, X. Yu, R. Lin, X. Bi, J. Lu, S. Bak, K.W. Nam, H.L. Xin, C. Jaye, D.A. Fischer, K. Amine, X.Q. Yang, Evolution of redox couples in Li- and Mn-rich cathode materials and mitigation of voltage fade by reducing oxygen release, Nat. Energy 3 (2018) 690–698.
[17] X.L. Xu, S.X. Deng, H. Wang, J.B. Liu, H. Yan, Research progress in improving the cycling stability of high-voltage LiNi0.5Mn1.5O4 cathode in lithium-ion battery, Nano-Micro Lett. 9 (2017) 22.
[18] K.M. Shaju, G.V. Subba Rao, B.V.R. Chowdari, Performance of layered Li(Ni1/3Co1/3Mn1/3)O2 as cathode for Li-ion batteries, Electrochim. Acta 48 (2002) 145–151.
[19] D. Aurbach, B. Markovsky, A. Rodkin, E. Levi, Y.S. Cohen, H.J. Kim, M. Schmidt, On the capacity fading of LiCoO intercalation electrodes:: the effect of cycling, storage, temperature, and surface film forming additives, Electrochim. Acta 47 (2003) 4291–4306.
[20] E.S. Lee, A. Manthiram, Smart design of lithium-rich layered oxide cathode compositions with suppressed voltage decay, J. Mater. Chem. A 2 (2014) 3932.
[21] F. Zheng, X. Ou, Q. Pan, X. Xiong, C. Yang, Z. Fu, M. Liu, Nanoscale gadolinium doped ceria (GDC) surface modification of Li-rich layered oxide as a high performance cathode material for lithium ion batteries, Chem. Eng. J. 334 (2018) 497–507.
[22] X. Zhang, I. Belharouak, L. Li, Y. Lei, J.W. Elam, A. Nie, X. Chen, R.S. Yassar, R.L. Axelbaum, Structural and electrochemical study of Al_2O_3 and TiO_2 coated Li1.2Ni0.13Mn0.54Co0.13O2 cathode material using ALD, Adv. Energy Mater. 3 (2013) 1299–1307.
[23] F. Wu, J. Liu, L. Li, X. Zhang, R. Luo, Y. Ye, R. Chen, Surface modification of Li-rich cathode materials for lithium-ion batteries with a PEDOT:PSS conducting polymer, ACS Appl. Mater. Interfaces 8 (2016) 23095–23104.
[24] D. Chen, W. Tu, M. Chen, P. Hong, X. Zhong, Y. Zhu, Q. Yu, W. Li, Synthesis and performances of Li-rich@AlF_3@graphene as cathode of lithium ion battery, Electrochim. Acta 193 (2016) 45–53.
[25] S. Guo, H. Yu, P. Liu, X. Liu, D. Li, M. Chen, M. Ishida, H. Zhou, Surface coating of lithium–manganese-rich layered oxides with delaminated MnO_2 nanosheets as cathode materials for Li-ion batteries, J. Mater. Chem. A 2 (2014) 4422.
[26] N. Yabuuchi, K. Kubota, Y. Aoki, S. Komaba, Understanding particle-size-dependent electrochemical properties of Li_2MnO_3-based positive electrode materials for rechargeable lithium batteries, J. Phys. Chem. C 120 (2016) 875–885.
[27] M.Y. Yang, S. Kim, K. Kim, W. Cho, J.W. Choi, Y.S. Nam, Role of ordered Ni atoms in Li layers for Li-rich layered cathode materials, Adv. Funct. Mater. 27 (2017) 1700982.
[28] J. Serrano-Sevillano, M. Reynaud, A. Saracibar, T. Altantzis, S. Bals, G. van Tendeloo, M. Casas-Cabanas, Enhanced electrochemical performance of Li-rich cathode materials through microstructural control, Phys. Chem. Chem. Phys. 20 (2018) 23112–23122.
[29] E.M. Erickson, H. Sclar, F. Schipper, J. Liu, R. Tian, C. Ghanty, L. Burstein, N. Leifer, J. Grinblat, M. Talianker, J.Y. Shin, J.K. Lampert, B. Markovsky, A.I. Frenkel, D. Aurbach, High-temperature treatment of Li-rich cathode materials with ammonia: improved capacity and mean voltage stability during cycling, Adv. Energy Mater. 7 (2017) 1700708.
[30] O.M. de Sousa, Study of the structural, electronic, and optical properties of the host matrices of $LiAl_5O_8$ and $LiGa_5O_8$ via DFT, Comput. Theor. Chem. 1123 (2018) 96–101.
[31] M. Mohapatra, M. Seshadri, Y.P. Naik, G. Meena, R.M. Kadam, V. Singh, Radiative properties of 'intense' red emitting $LiAl_5O_8$: Eu phosphors, J. Mater. Sci. Mater. Electron. 29 (2018) 7778–7784.
[32] M. Aykol, S. Kim, V.I. Hegde, D. Snydacker, Z. Lu, S. Hao, S. Kirklin, D. Morgan, C. Wolverton, High-throughput computational design of cathode coatings for Li-ion batteries, Nat. Commun. 7 (2016) 13779.
[33] Y. Xie, S. Chen, W. Yang, H. Zou, Z. Lin, J. Zhou, Improving the rate capability and decelerating the voltage decay of Li-rich layered oxide cathodes by constructing a surface-modified microrod structure, J. Alloy. Comp. 772 (2019) 230–239.
[34] L. Li, Z. Chen, Q. Zhang, M. Xu, X. Zhou, H. Zhu, K. Zhang, A hydrolysis-hydrothermal route for the synthesis of ultrathin $LiAlO_2$-inlaid LiNi0.5Co0.2Mn0.3O2 as a high-performance cathode material for lithium ion

batteries, J. Mater. Chem. A 3 (2015) 894–904.
[35] Y. Su, Y. Yang, L. Chen, Y. Lu, L. Bao, G. Chen, Z. Yang, Q. Zhang, J. Wang, R. Chen, S. Chen, F. Wu, Improving the cycling stability of Ni-rich cathode materials by fabricating surface rock salt phase, Electrochim. Acta 292 (2018) 217–226.
[36] S.W. Woo, S.T. Myung, H. Bang, D.W. Kim, Y.K. Sun, Improvement of electrochemical and thermal properties of Li[Ni0.8Co0.1Mn0.1]O2 positive electrode materials by multiple metal (Al, Mg) substitution, Electrochim. Acta 54 (2009) 3851–3856.
[37] C. Ye, W. Tu, L. Yin, Q. Zheng, C. Wang, Y. Zhong, Y. Zhang, Q. Huang, K. Xu, W. Li, Converting detrimental HF in electrolytes into a highly fluorinated interphase on cathodes, J. Mater. Chem. A 6 (2018) 17642–17652.
[38] M.J. Lee, E. Lho, P. Oh, Y. Son, J. Cho, Simultaneous surface modification method for 0.4Li2MnO3-0.6LiNi1/3Co1/3Mn1/3O2 cathode material for lithium ion batteries: acid treatment and $LiCoPO_4$ coating, Nano Res. 10 (2017) 4210–4220.
[39] S. Yang-Kook, L. Min-Joon, S. Chong, Yoon, H. Jusef, A. Khalil, S. Bruno, The role of AlF_3 coatings in improving electrochemical cycling of Li-enriched nickel-manganese oxide electrodes for Li-ion batteries, Adv. Mater. 24 (2012) 1192–1196.
[40] H. Konishi, T. Hirano, D. Takamatsu, A. Gunji, X. Feng, S. Furutsuki, T. Okumura, S. Terada, K. Tamura, Mechanisms responsible for two possible electrochemical reactions in Li1.2Ni0.13Mn0.54Co0.13O2 used for lithium ion batteries, J. Solid State Chem. 258 (2018) 225–231.
[41] K. Mu, Y. Cao, G. Hu, K. Du, H. Yang, Z. Gan, Z. Peng, Enhanced electrochemical performance of Li-rich cathode Li1.2Ni0.2Mn0.6O2 by surface modification with WO_3 for lithium ion batteries, Electrochim. Acta 273 (2018) 88–97.
[42] J. Liu, B. Reejajayan, A. Manthiram, Conductive surface modification with aluminum of high capacity layered Li[Li0.2Mn0.54Ni0.13Co0.13]O2 cathodes, J. Phys. Chem. C 114 (2010) 9528–9533.